Cancer Nanotechnology

RESEARCH Open Access

Histopathology, pharmacokinetics and estimation of interleukin-6 levels of *Moringa oleifera* leaves extract-functionalized selenium nanoparticles against rats induced hepatocellular carcinoma

Eman M. M. Ebrahem[1], Galal H. Sayed[1], Gehan N. A. Gad[2], Kurls E. Anwer[1] and Adli A. Selim[3*]

*Correspondence: adli_a_selim@yahoo.com

[3] Labeled Compounds Department, Hot Laboratories Centre, Egyptian Atomic Energy Authority (EAEA), Cairo 13759, Egypt
Full list of author information is available at the end of the article

Abstract

Background: Hepatocellular carcinoma (HCC) is one of the most dangerous cancers in all the world. This study focused on prevention and therapy of hepatocellular carcinoma (HCC) using *Moringa oleifera* extract combined with vitamin C and selenium in a nanoplatform (MO/asc.-Se-NPs).

Results: Full characterization of MO/asc.-Se-NPs was performed by using different analytical techniques (TEM, DLS, zeta-sizer), and its antioxidant capacity was measured by DPPH assay. Biodistribution study was performed with the aid of radiolabeling technique using technetium-99m in normal albino mice. HCC was induced in Wister albino rats to evaluate the efficiency of MO/asc.-Se-NPs in the treatment of HCC. The biomarker analysis (ALT, AST and ALB) shows improvement in its values in prevention and treated groups by using MO/asc.-Se NP. The levels of inflammatory marker interleukin 6 (IL6 tissue homogenate) was improved by decreasing its values in these two groups also. Histology section of tissue liver showed alleviation in treated and prevention groups.

Conclusions: In conclusion, MO/asc.-Se-NPs can be used as a potential agent for prevention and treatment of HCC after further preclinical studies.

Keywords: *Moringa oleifera*, Se-NPs, Hepatocellular carcinoma, Interleukin-6, ^{99m}Tc-complexation

Background

Hepatocellular carcinoma (HCC) is one of the most dangerous cancers in all the world which represents the third fundamental reason of death with 700,000 annual death (Choi et al. 2022), many factors that lead to hepatocellular carcinoma (HCC) malignant tumors in humans. The most important are HCV (hepatitis C virus), chronic HBV (hepatitis B virus), diabetes mellitus, obesity and chronic alcohol use (Aljuhr et al. 2021;

Choi et al. 2022), There are some chemicals that causes deep injury in liver and advancement of tumors as compounds act as genotoxic agents which stimulated formation of tumor and other compound that represented promoting agents if it taken with genotoxic agents causes immediately tumor figuration (Shamsel-Din et al. 2020). Promoting agents demonstrated to expedite the clonal amplification of the preneoplastic which directly raises tumor progress (Muriel, 2009) the symptoms of HCC can be observed through abdominal pain, enlarged abdomen, hemorrhage and yellow skin or eyes (jaundice) (Schacherer et al. 2007). Natural products found in many sources plants, marine organisms and microorganisms which have a diverse biological activities (Katz et al. 2016) are considered a valuable source of many chemical structures that used for drug discovery and pharmaceutical purpose (Newman and Cragg 2020) from ancient times, a different diseases as malaria, immune and cancer can be treated by using natural product natural product and their derivatives (Tajuddeen et al. 2019). Medicinal plants one of the natural product resources that give it a huge value for its economical, industrial, environmental and pharmaceutical applications for human life (Nazir and Gangoo 2022; Sharma et al. 2021; Yeshi et al. 2022). *Moringa oleifera* (*MO*) is a tree of species belongs to family of *Moringaceae* found in Himalayan and sub-Himalayan regions such as tropical and subtropical countries as India, Bangladesh, Afghanistan and Pakistan (Moichela 2021; Okorie et al. 2019). *MO* has wide range applications in medicine and many other fields which rightly earned the nickname drumstick tree (de Siqueira Patriota et al. 2020; Meireles et al. 2020). Leaves of *MO* have a good supply of many vitamins (Fig. 1) for example vitamin A (Brar et al. 2022; MGBOJIKWE et al. 2022) that is important for vision problems, embryonic growth, immune reproduction, and cell differentiation (Susanto et al. 2019), presence of vitamin C about 200 mg/100 g that considered a high concentration that found in oranges (Akhter 2023; Wijaya 2019) also vitamin E one of compositions of moringa with concentration that found in nuts (Rodriguez 2020; Salama et al. 2020) which give moringa a great value because its antioxidant and inhibit cell proliferation (Gong et al. 2018; Safitri et al. 2022). *MO* leaves also protect the body from various deleterious effects of free radicals, pollutants and toxins and act as antioxidants (Soliman et al. 2021). *MO* is a good source to polyphenol compounds as phenolic acids and flavonoids, which have been synthesized in plant in response to antimicrobial infections that contain a benzo-pyrone ring (Fontana et al. 2022), flavonoids demonstrated a great results in treatment some of chronic diseases like cardiovascular disease and cancer (Ati et al. 2022; Ciumărnean et al. 2020). It was found that myricetin, quercetin and kaempferol (Fig. 1) are the largest concentration of flavonoids in moringa (Vonghirundecha et al. 2022). Oxidative stress activates inflammatory pathways leading to transformation of a normal cell to tumor cell, tumor cell, all observations to date suggest that oxidative stress, chronic inflammation, and cancer are closely linked (Dutta et al. 2021; Zhou et al. 2021). Antioxidants can disrupt the formation of free radicals and reduce oxidative stress, which ultimately prevents cancer (Akbari et al. 2022). *MO* leaves contain some vital compounds such as rutin, gallic acid, coumaric and quercetin which contain antioxidants which they have important role as antioxidant and reduced oxidant stress due to scavenger for nitric oxide radicals and has a potential source of natural antioxidant (Pereira et al. 2021); whereas, ascorbic acid (vitamin C) has multi-biological benefits that enhance the protection against endothelia dysfunction, carcinogenicity (Elbakry et al.

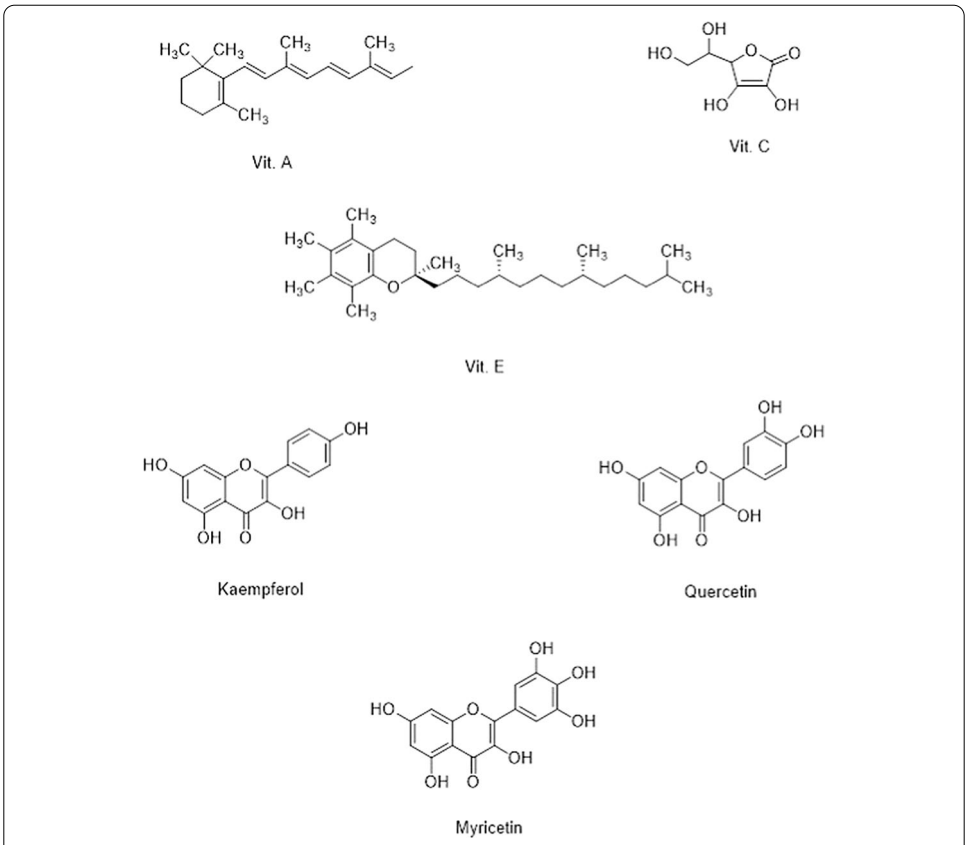

Fig. 1 Some active components of *MO* leaves extract

2019). Nanomaterials have a long list of applicability in improving human life and its environment. Noble nanoparticles have been synthesized for biotechnology, electronics and environmental purposes (Alsohaimi et al. 2020) one of the methods used for synthesis of nanoparticles is green chemistry environment friendly represented in plants because of its benefits as overcomes the disadvantage of chemical and physical method which toxic chemicals, energy, pressure and temperature are no longer needed (Thomas et al. 2020). Bioavailability is the amount and rate of drug absorption. The absorption rate is desired to be fast or slow according to the treatment conditions which can be achieved by altering the drug's physicochemical properties and the dosage form characteristics. The nano-formulation has many advantages, especially in phytomedicine including bioavailability improvement, decreasing toxicity, pharmacological activity enhancement, etc. (Chung et al. 2018). So, the nano-phytomedicine has a high potential future for activity improvement and overcoming problems associated with herbal drugs. Selenium (Se) confirmed that is very important for human dietary supply because of vital part in some antioxidant enzymes which has a role in protecting against cellular damage in tissues that at the long-term causes dangerous diseases (Korany et al. 2020; Sakr et al. 2018). Selenium nanoparticles (Se-NPs) are one of selenium forms that are considered a lower toxicity and better biocompatibility (Bai et al. 2017). Se-NPs have a great vital prospect in medical studies, particularly therapy approaches, like anti-malignancy against some types of cancers (Nie et al. 2016), synergism with other drugs

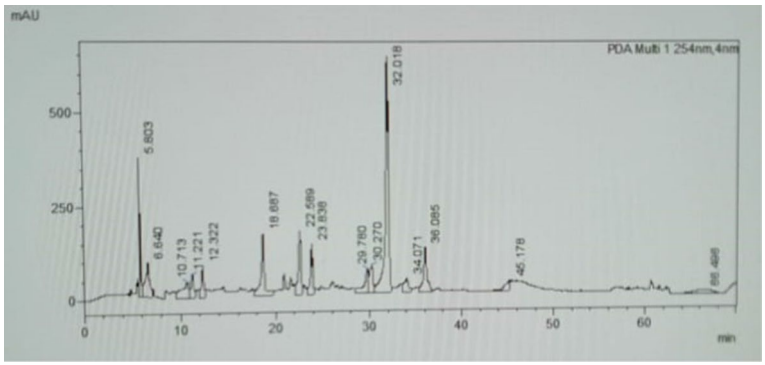

Fig. 2 HPLC chromatogram of *MO* methanolic

Table 1 Phenolic profile in *MO* extract

Compound	Conc. (mg/g extract)
Gallic	0.126
p-Hydroxybenzoic	1.567
Catechin	0.732
Chlorogenic	0.045
Caffeic	0.551
Syringic	0.106
Ferulic	0.247
Sinapic	0.016
p-Coumaric	0.342
Rutin	4.402
Quercetin	0.018
Kaempferol	0.011

(Li et al. 2018), drug delivery (Xia et al. 2019) antiinflammation (Malhotra et al. 2016) and immune-stimulation (Menon et al. 2018). We aimed in this study- to synthesis a novel nano-complex to be used for the treatment of HCC depending on the synergistic effect of selenium and *MO* components using additional amount of vitamin C (*MO*/asc.-Se-NPs).

Results and discussion

HPLC analysis of *M. oleifera* methanolic extract

HPLC-assay of flavonoids and phenolic compounds is presented in Fig. 2. The phenolic compounds identified in *MO* (Table 1) that showed the highest concentrations were rutin: 4.402 mg/1 g methanol extract, p-hydroxybenzoic: 1.567 mg/1 g and quercetin: 0.018 mg/1 g dry extract, while the lowest phenolic compounds concentration identified in *MO* were sinapic: 0.16 mg/1 g and kaempferol. 0.011 mg/1 g dry extract.

Synthesis and characterization of *MO*/asc.-Se-NPs

Selenium, Vit. C and MO are well-known potential antioxidants. Vit. C was used as a reducing agent to form selenium particles from selenium ions and also it is used to stabilize the formed nanoparticles through the prevention of aggregation of selenium nanoparticles. Then the formed asc.-Se-NPs were functionalized using *MO* extract forming *MO*/asc.-Se-NPs. *MO*/asc.-Se-NPs average size were determined using different techniques (TEM and DLS) (Essa et al. 2020; Fayez et al. 2020) (Fig. 3). TEM shows spherical shape NPs with mean diameter 30 nm; while DLS shows 211.8 average hydrodynamic diameter and its stability appeared by measuring zeta-potential giving 36.6 mV indicating the stability of the colloidal *MO*/asc.-Se NPs. This stability may be due to the presence of charged surface which creates electrostatic repulsion (Sakr et al. 2020).

Antioxidant capacity MO /asc.-Se-NPs

The one of main causes of DNA damage is free radicals that represent the first stage of carcinoma (Johnson 2007). Natural products consist of many of antioxidant source acting exogenously which stimulates function of the endogenous antioxidant system to prevent free radicals formation inside the body as its main responsibility. *Moringa oleifera* leaves are rich in antioxidant compounds which represent in flavonoids and phenolic

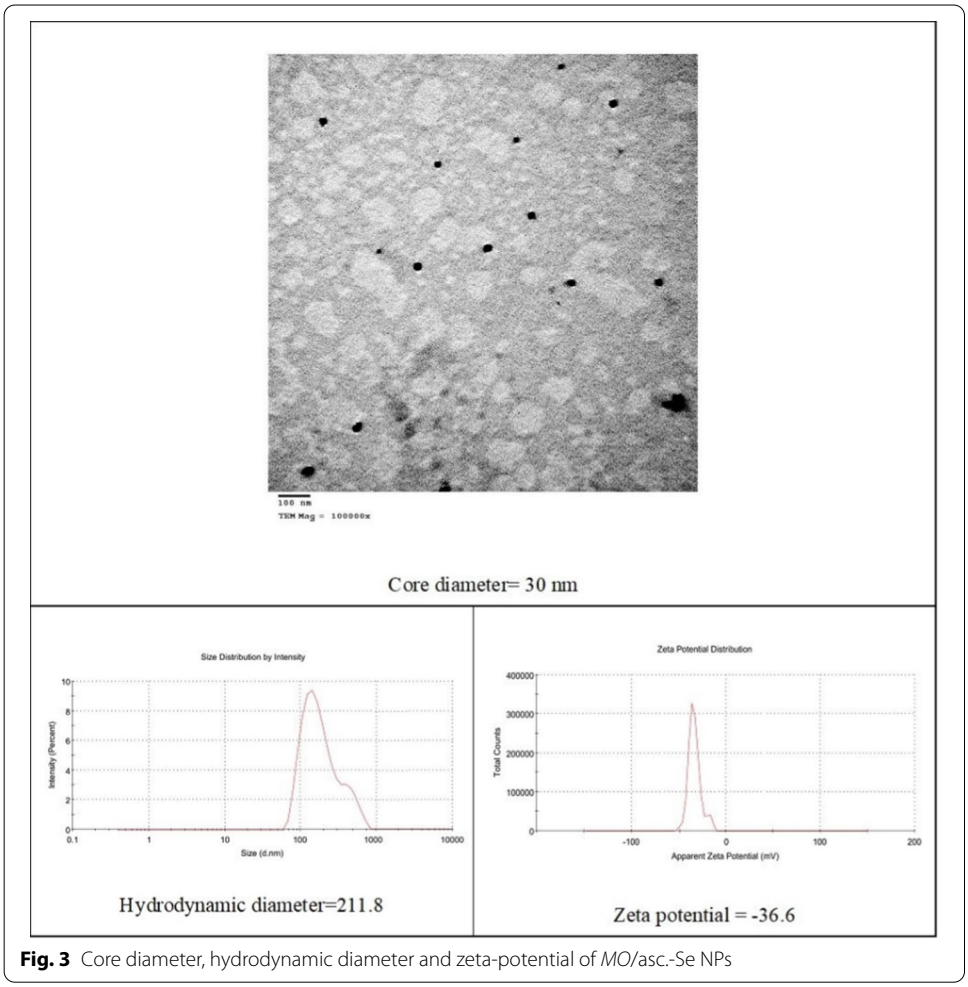

Fig. 3 Core diameter, hydrodynamic diameter and zeta-potential of *MO*/asc.-Se NPs

constituents as of gallic acid, quercetin and kaempferol (Leone et al. 2016) which increased its value to overcome and prevent many diseases such as inflammation and cancers (Fitriana et al. 2018).

a) DPPH assay

MO/asc.-Se-NPs showed the highest scavenging activity with IC_{50} of 3.79±0.87 µL/mL followed by ascorbic acid with IC_{50} of 8.05±0.50 µL/mL, while the value of IC_{50} for both selenium and moringa ext. >1000.

b) Superoxide dismutase (SOD)

Superoxide anion radical scavenging activity *MO*/asc.-Se-NPs exhibited potent scavenging activity for superoxide anion radical. The IC_{50} value of superoxide anion radical scavenging capacity for *MO*/asc.-Se-NPs, ascorbic acid, selenium, and moringa extract were found to be 6.11±1.26, 12.25±1.03, > 1000 and > 1000 µL/mL, respectively

Radiolabeling of *MO*/asc.-Se-NPs

The optimization study for RCP of [^{99m}Tc]Tc-*MO*/asc.-Se-NPs was carried out by studying Sn(II), *MO*/asc.-Se-NPs, pH and the reaction time at room temperature. The higher RCP (97.2%) was obtained by using 10 µg Sn (II), 1 mL *MO*/asc.-Se-NPs at pH 5 after 20 min. The amount of reducing agent (Sn (II)) is the most effective factor in the % RCP determination study. Without the reducing agent, ^{99m}Tc in the form of $^{99m}TcO_4^-$ unable to chelate with any agent. At low amounts of Sn (II) the free ^{99m}Tc was high due to the insufficient amount to reduce all pertechnetate in the solution; but at high amount R-H ^{99m}Tc (reduced-hydrolyzed technetium) become high due to the formation of colloid impurities (Motaleb et al. 2018) (Fig. 4). As clearly noticed from Fig. 5 the high amount of *MO*/asc.-Se-NPs has no significant effect at % RCP; while at amounts lower than the optimum the % RCP was low due to insufficient amount to chelate with the all reduced ^{99m}Tc. At slightly acidic pH (pH 5) the higher RCP was obtained; but at lower or higher

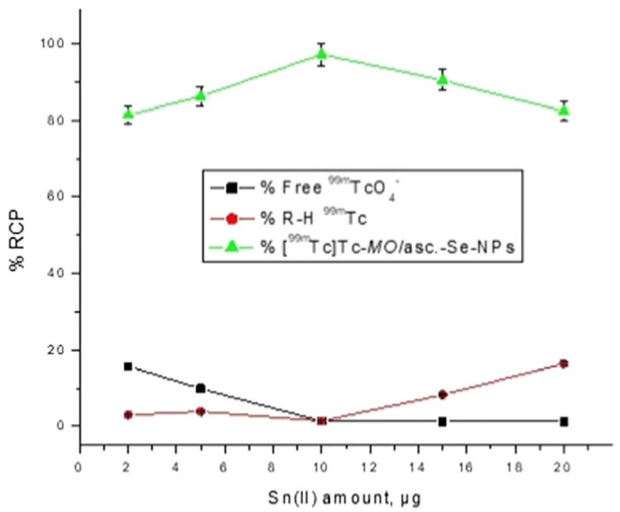

Fig. 4 Effect of Sn(II) amount, µg (% RCP ± SD, $n = 3$)

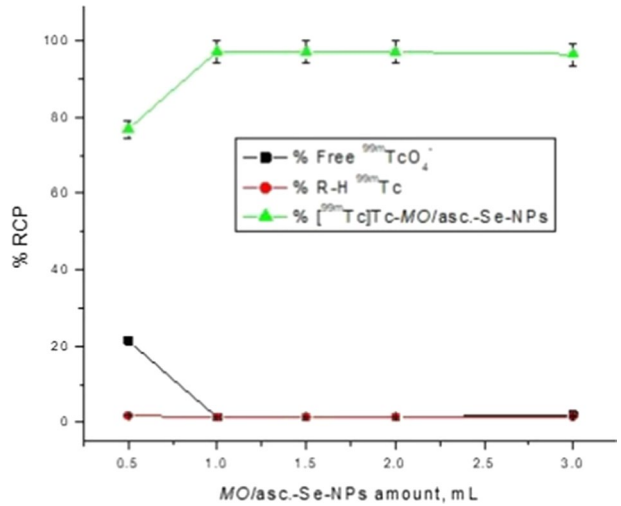

Fig. 5 Effect of substrate amount, Ml (% RCP ± SD, $n = 3$)

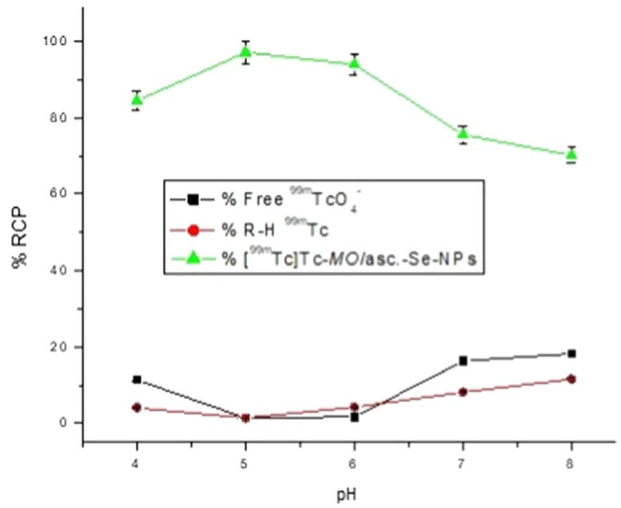

Fig. 6 Effect of pH (% RCP ± SD, $n = 3$)

this value % RCP was decreased (Fig. 6). The reaction of ^{99m}Tc with *MO*/asc.-Se-NPs was fast and the optimum yield was obtained after 20 min only and when the reaction still at room temperature, the % RCP still stable which indicates the stability of the formed complex [^{99m}Tc]Tc-*MO*/asc.-Se-NPs (Fig. 7).

Pharmacokinetic study of [^{99m}Tc]Tc-*MO*/asc.-Se-NPs complex

The biodistribution of nanoparticles in normal mice mainly depended on both the particles size and the functionalized surface (Augustine et al. 2020). The biodistribution of [^{99m}Tc]Tc-*MO*/asc.-Se-NPs is clarified in Fig. 8**.** The high uptake in liver was clearly appeared; while there is no specific uptake in the thyroid or stomach which indicates the in vivo stability of [^{99m}Tc]Tc-*MO*/asc.-Se-NPs. The uptake ratio in liver started from

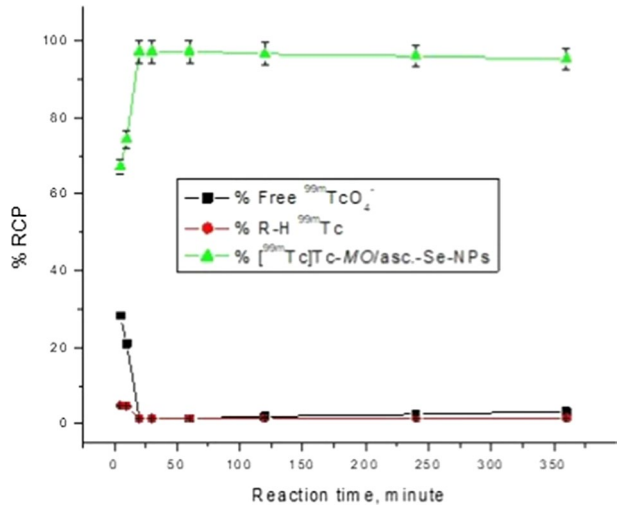

Fig. 7 Effect of reaction time, min (% RCP ± SD, $n = 3$)

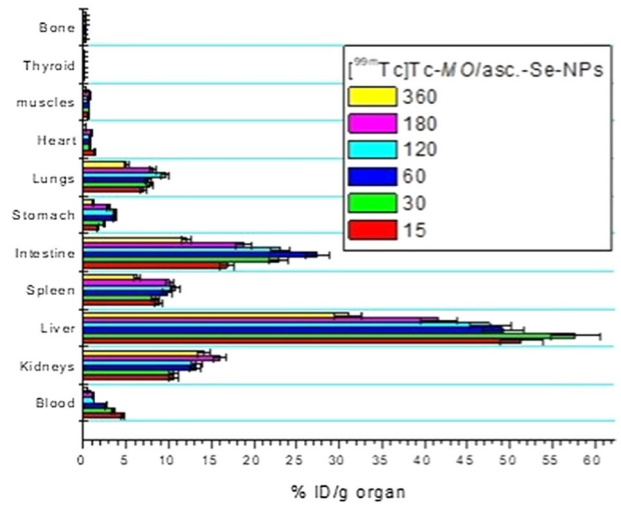

Fig. 8 Biodistribution study of [^{99m}Tc]Tc-*MO*/asc.-Se-NPs complex (% ID/g ± S.D, $n = 3$)

51.35 to 31.01% ID/g after 15 and 360-min post-injection, respectively. This high uptake in liver may be due to the anti-HCC of *MO*/asc.-Se-NPs and its size. The ability of the liver to gain high quantity from *MO*/asc.-Se-NPs platform can increase the power of this platform to be preventive and treatment agent for HCC.

Biochemical study

HCC-induced rats (group 3) showed significantly ($p < 0.05$) higher levels of liver enzyme ALT, AST and Alb where the results were 102 ± 3.06 U/L, 286 ± 8.58 U/L and 2.59 ± 0.07 mg/dl, respectively, compared with other groups while in preventive group 4 showed lower level of ALT, AST and Alb than group 3, 80 ± 2.40 U/L, 156 ± 4.68 U/L and 3.23 ± 0.10 mg/dl, respectively, and in treatment group 5 with *MO*/asc.-Se-NPs

observed more improvement in liver enzymes and albumin with results 69 ± 2.07 U/L, 138 ± 4.14 U/L and 3.46 ± 0.11 mg/dl, respectively (Table 2).

Table 2. Results of liver function analysis of the five experimental groups

Groups	ALT, U/L	AST, U/L	Alb, mg/dl
1	38 ± 1.14	96 ± 2.88	3.70 ± 0.11
2	71 ± 2.13	151 ± 4.53	3.46 ± 0.10
3	102 ± 3.06	286 ± 8.58	2.59 ± 0.07
4	80 ± 2.40	156 ± 4.68	3.23 ± 0.10
5	69 ± 2.07	138 ± 4.14	3.46 ± 0.11

*(mean ± SD, $n = 3$, $P < 0.05$)

Liver enzymes ALT, AST and Alb are considered as the biomarkers of hepatic cellular damage which ALT found predominantly in liver which increases in its rate were evidence of liver injury (Fakurazi et al. 2008) while AST is a biomarker for diagnosis amino acid metabolism and myocardial infarction (Ghosh et al. 2010). These enzymes are present in mitochondria, cytoplasm and released in circulation after loss of functional integrity of cell membrane and cellular leakage (Lahkar et al. 2012) and Alb is type of protein that is formed in liver and functions in keeping the fluid in bloodstream and preventing leakage into other tissues and it carries different substances such as hormones, enzymes and vitamins, and any disturbance in liver leads to decreased serum albumin concentration in the blood, (Garcia-Martinez et al. 2013) Alb has binding functions, such as ABiC and albumin metal ion binding capacity, were significantly lower in several liver diseases, including cirrhosis and liver failure (Domenicali et al. 2014) in our study *MO*/asc.-Se-NPs was considered a novel nano-drug depended on natural products containing many metabolites such as polyphenols, flavonoids and saponins which act as antioxidant improvement in liver function test (Choudhari et al. 2020) that was shown in preventive and treatment groups.

Antioxidants and lipid peroxidation

Table 3 shows the effect of treatment on the experimental groups that through it the infected HCC group 3 noticed the highest significantly lipid peroxidation (as measured by malondialdehyde "MDA") in liver tissue homogenate compared to other groups with rate 447.49, while preventive group 4 and treatment group 5 observed a significantly decreased in MDA with levels 243.80 and 157.24, respectively. Many researches have been proved that CCl_4 induced the hepatotoxic which increased lipid peroxidation and

Table 3 Effect of *MO*/asc.-Se-NPs administration on liver homogenate MDA concentration

Serial	Code	MDA concentration (nmol/g tissue)
1	G1	126.99
2	G2	226.83
3	G3	447.49
4	G4	243.80
5	G5	157.24

*(mean ± SD, $n = 3$, $P < 0.05$)

decreased antioxidants presence of some vital compounds rutin, gallic acid, coumaric and quercetin in *MO* leaves which they have important role as antioxidant and reduced oxidant stress due to scavenger for nitric oxide radicals and has a potential source of natural antioxidant; whereas (vitamin C) ascorbic acid have multi-biological benefits that enhance the protection against endothelia dysfunction, carcinogenicity (Elbakry et al. 2019).

Inflammatory markers interleukin-6 (IL-6)

As presented in Table 4, increasing in interleukin-6 in HCC group 3 with 1030.3 compared with other experimental groups while in preventing group 4 and treatment groups 5 noticed a significantly decrease in the rate of IL-6 with 522.1 and 429.5, respectively. IL-6 one of cytokines that are messenger molecules of the immune system, mediating cellular movement among lymphocytes, macrophages, dendritic cells, and other inflammatory cells act as inflammatory biomarkers in chronic hepatitis which activate local inflammatory, activated Kupffer cells and hepatocyte proliferation leading to cancerous hepatocytes (Naugler and Karin 2008) in first stage of HCC development IL-6 induced the growth of irregular hepatocytes leading to gathering damage of DNA and increased β-catenin activation moreover consequently to carcinogenesis and progress the tumor growth (Bergmann et al. 2017). Natural product which represented in *MO* leaves riches with antioxidant that succeeded in lessen inflammatory effect and decreased the level of IL-6 (Bhondave et al. 2014) it can be said to show profound influence on inflammatory-associated diseases and resultant symptoms. On the basis of our study, it can be postulated that *MO*/asc.-Se-NPs can exert its hepatoprotective effect and anti-inflammatory action against these cytokines.

Histopathological effect of *Moringa oleifera* on the hepatic structure of rats

Carbon tetrachloride is a strong hepatotoxic compound which is used widely in to induce hepatocellular injury (Al-Sayed et al. 2019). CCL_4 ROS (generates reactive oxygen species) which may induce hepatic inflammation via Kupffer cells stimulation which generate proinflammatory mediators such as interleukins and COX-2, and several ROS. Furthermore, radicals that generate from CCL_4 can initiate oxidative stress, lipid peroxidation, DNA damage, necrosis of the liver (Lin et al. 2012). TAA was used for induction of fibrosis, cirrhosis, and liver cancer. Its toxicity mechanisms may be

Table 4 Effect of *MO*/asc.-Se-NPs administration on liver homogenate IL-6

Serial	Codes	IL-6 concentration (pg./mL)
1	G1	324.6
2	G2	429.5
3	G3	1030.3
4	G4	522.1
5	G5	460.8

*(mean ± SD, $n = 3$, $P < 0.05$)

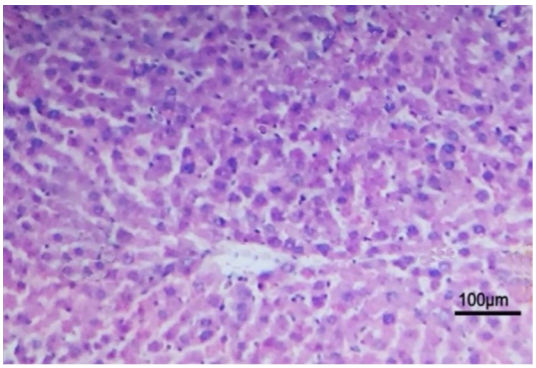

Fig. 9 Photomicrograph of H&E-stained rat liver of control group (1) at 84th day showing normal tissue architecture and cellular details (scale bar = 100 µm)

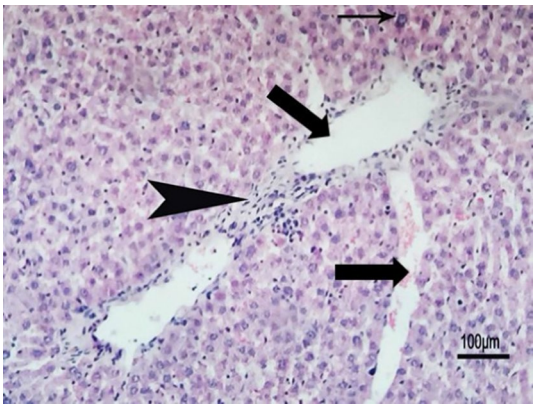

Fig. 10 Photomicrograph of H&E-stained rat liver of group (2) at 84th day showing mild perivascular infiltration with Von Kupffer cells and fibroblast (arrowhead) (scale bar = 100 µm)

due to its oxidant properties (Kornek et al. 2006). The microscopic examination of the tested groups of liver tissue samples is shown in Figs. 9, 10, 11, 12, 13, 14, 15, 16, 17, 18, 19, 20, 21, 22, 23.

- Group 1 (normal control group) displayed normal liver tissue architecture, cellular details, intact subcapsular tissue, hepatocytes with intact hepatic vasculatures and portal areas with intact hepatic sinusoids (Fig. 9).
- Group 2 (*MO*/asc.-Se-NPs supplement) Showed some reversible mild degenerative changes in some rats as mild perivascular leucocytic cellular infiltration with Von Kupffer cells and fibroblast cells with diffuse hydropic degeneration of hepatocytes (Fig. 10). Some other rats showed apparent intact morphological features resembling normal control samples without abnormal pathological changes. Few rats revealed diffuse hydropic degeneration of hepatocytes (Fig. 11).
- Group 3 (hepatic carcinoma induction group without any treatment) showed severe liver lesions in all experimental rats ranged from inflammation, fibrosis till carcinomas induction. Severe congestion of hepatic blood vessels with focal areas of dilated

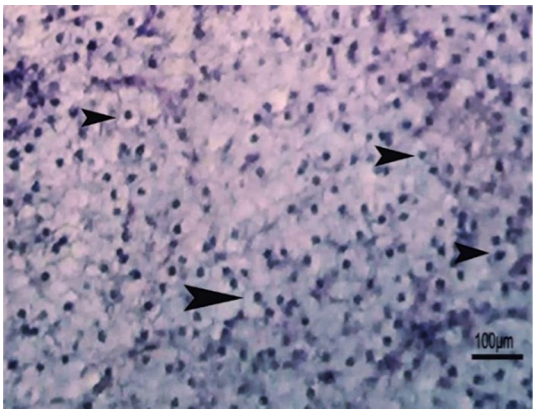

Fig. 11 Photomicrograph of H&E-stained rat liver of group (2) at 84th day showing diffuse hydropic degeneration of hepatocytes (arrowhead) (scale bar = 100 µm)

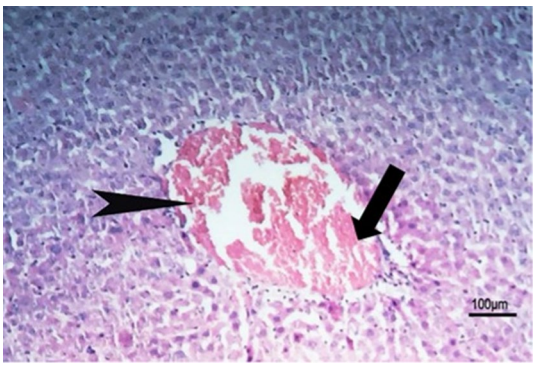

Fig. 12 Photomicrograph of H&E-stained rat liver of group (3) at 84th day showing severe congestion of hepatic blood vessels (arrowhead) with focal area of dilated sinusoids (scale bar = 100 µm)

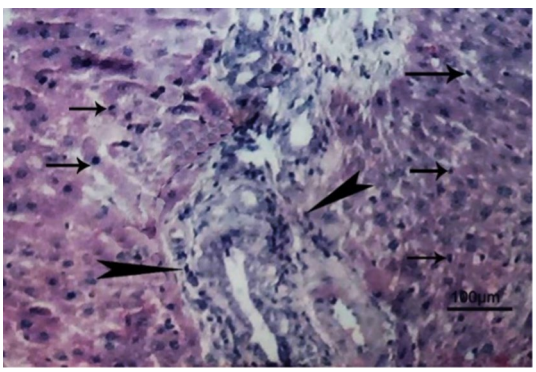

Fig. 13 Photomicrograph of H&E-stained rat liver of group (3) at 84th day showing severe periductal fibrosis (arrowhead) with diffuse infiltration of von Kupffer cells (arrows) (scale bar = 100 µm)

sinusoids were clear in all examined livers (Fig. 12). Diffuse loss of both tissue architecture, cells boundaries and details were detected in most liver samples. Some rats' livers exhibited severe periductal fibrosis with diffuse infiltration of von Kupffer cells

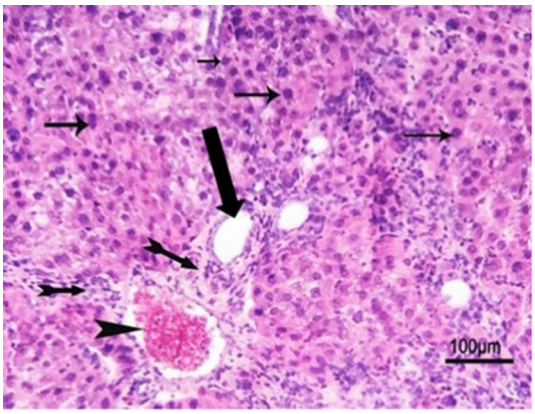

Fig. 14 Photomicrograph of H&E-stained rat liver of group (3) at 84th day showing focal areas of hyperchromatic divided nuclei with loss of cellular details and tissue architecture (arrows), severe congestion of hepatic blood vessel (arrowhead) and periductal fibrosis (scale bar = 100 µm)

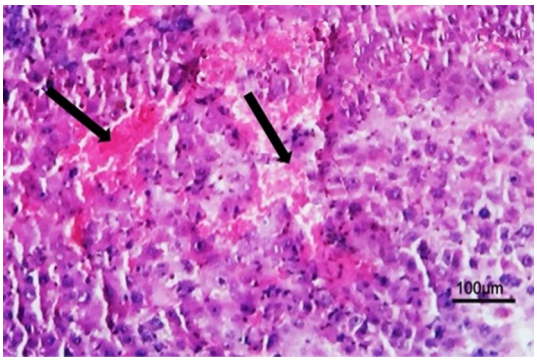

Fig. 15 Photomicrograph of H&E-stained rat liver of group (3) at 84th day showing severe diffuse hemorrhage with diffuse hyperchromatic divided nuclei with loss of cellular details and tissue architecture (scale bar = 100 µm)

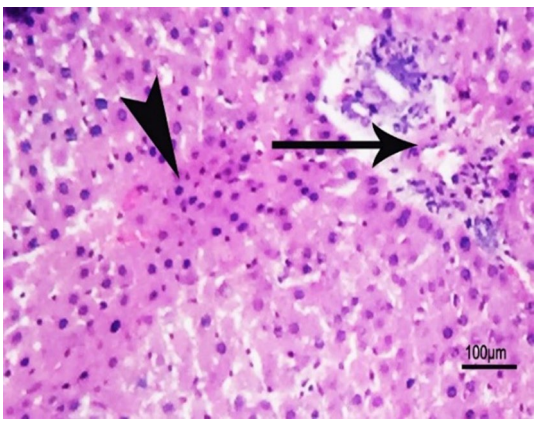

Fig. 16 Photomicrograph of H&E-stained rat liver of group (3) at 84th day showing focal area of divided hepatocytes(arrowhead)with periductal fibrosis and edema(arrow) (scale bar = 100 µm)

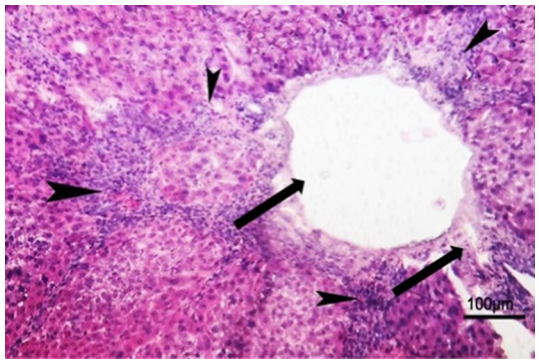

Fig. 17 Photomicrograph of H&E-stained rat liver of group (3) at 84th day showing severe perivascular fibrosis (arrowhead) with hepatocellular carcinoma (HCC) grade II represented in loss of hepatic tissue architecture with cellular and nuclear pleomorphism and missed polarity (scale bar = 100 µm)

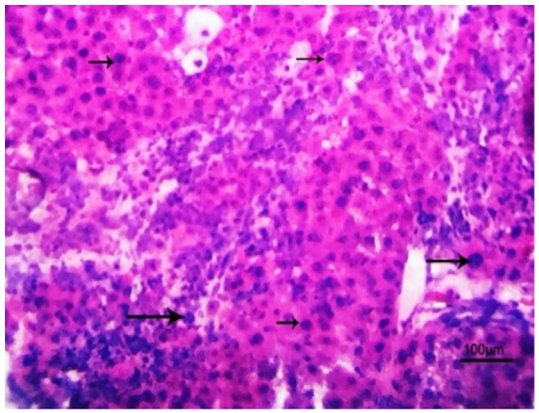

Fig. 18 Photomicrograph of H&E-stained rat liver of group (3) at 84th day showing diffuse divided hepatocytes (arrow)with hyperchromatic nuclei (scale bar = 100 µm)

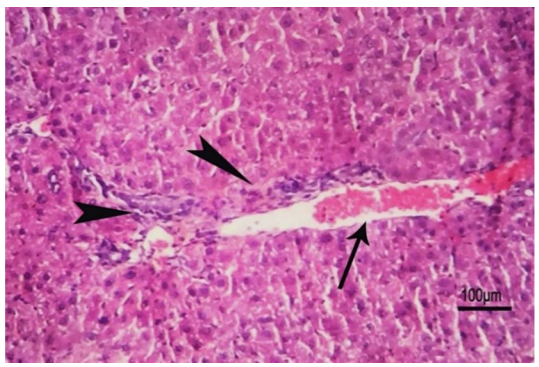

Fig. 19 Photomicrograph of H&E-stained rat liver of group (4) at 84th day showing mild perivascular infiltration with fibroblast cells (arrowhead) with congestion(arrow) (scale bar = 100 µm)

(Fig. 13) with or without focal areas of hyperchromatic divided nuclei with loss of cellular details and tissue architecture (Fig. 14). Few rats' livers showed severe diffuse hemorrhage, diffuse hyperchromatic divided nuclei with loss of cellular details

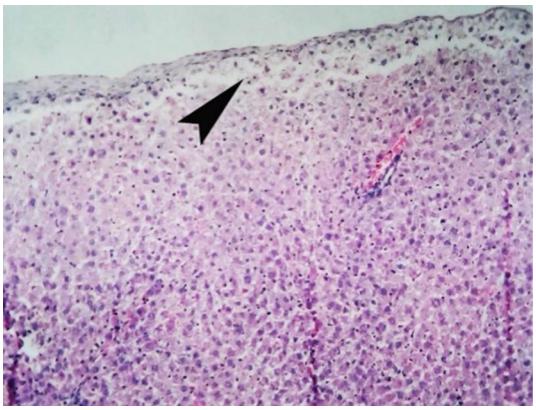

Fig. 20 Photomicrograph of H&E-stained rat liver of group (4) at 84th day showing subcapsular atrophy of hepatocytes with (scale bar = 100 µm)

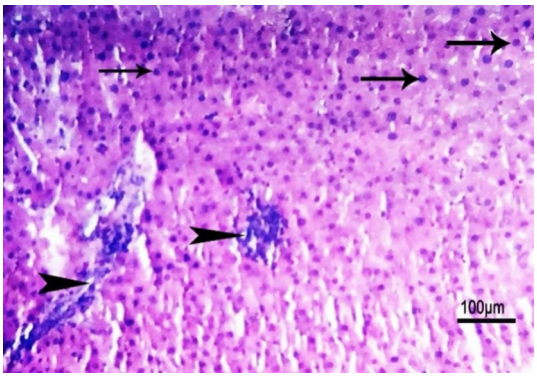

Fig. 21 Photomicrograph of H&E-stained rat liver of group (4) at 84th day showing focal areas of lymphocytes cellular infiltration (arrowhead) with sporadic areas of hyperchromatic divided nuclei (arrows) (scale bar = 100 µm)

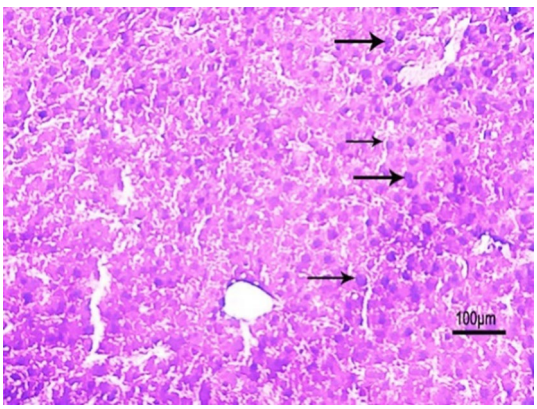

Fig. 22 Photomicrograph of H&E-stained rat liver of group (5) at 112th day showing restricted small areas of hyperchromatic divided nuclei (arrows) within normal hepatic parenchyma (scale bar = 100 µm)

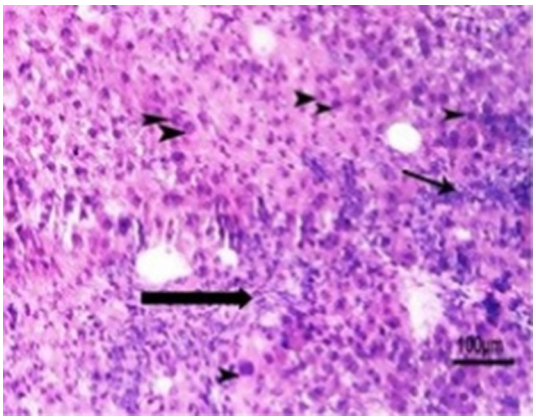

Fig. 23 Photomicrograph of H&E-stained rat liver of group (5) at 112th day showing sporadic areas of hyperchromatic divided nuclei (arrowhead) with loss of tissue architecture and cellular details in addition to fibrosis and cellular infiltration (arrow) (scale bar = 100 µm)

and tissue architecture perivascular fibrosis with hepatocellular carcinoma (HCC) grade II represented in loss of hepatic tissue architecture with cellular and nuclear pleomorphism and missed polarity (Fig. 15). Focal areas of divided hyperchromatic hepatocytes with periductal fibrosis and edema were observed (Fig. 16). Some cases exhibited severe perivascular fibrosis (arrowhead) with hepatocellular carcinoma (HCC) grade II represented in loss of hepatic tissue architecture with cellular and nuclear pleomorphism and missed polarity (Fig. 17). Severe diffuse divided hyperchromatic nuclei of hepatocytes were very clear in some cases (Fig. 18).

- Group 4 (prevention group) Mild-to-moderate lesions were noticed while few cases showed early carcinomas development. Some rats' livers showed mild perivascular infiltration with fibroblast cells with congestion of hepatic blood vessels (Fig. 19). Subcapsular atrophy of hepatocytes was also observed in some other cases (Fig. 20). Few rats' livers exhibited focal areas of lymphocytes cells infiltration with sporadic areas of hyperchromatic divided nuclei of hepatocytes (Fig. 21). The mechanism of the hepatoprotective activity was shown to be related to the scavenging free radicals because phenolic compounds exhibited strong antioxidant activity (Al-Sayed et al. 2019; Shimoda et al. 2008)
- Group 5 (*MO*/asc.-Se-NPs drug treatment) Few rats' livers showed sporadic restricted areas of hyperchromatic divided nuclei (Fig. 22) with almost maintained tissue architecture and cellular details in addition to fibrosis and cellular infiltration and other rats showed tissue improvements and diminished lesions through showed only few reversible degenerative changes as diffuse hydropic degeneration of hepatocytes in the hepatic parenchyma. Other few cases showed restricted small areas of hyperchromatic divided nuclei with loss of tissue architecture and cellular details in addition to fibrosis and cellular infiltration (Fig. 23).

The hepatoprotective effect of the newly synthesized nanoplatform may be due to its power to guard the liver against the induced pathological changes. Generally, the control

group displayed normal liver tissue compared with other groups while in (MO /asc.-Se-NPs drug supplement) Group 2 noticed mild perivascular infiltration with Von Kupffer cells and fibroblast with diffuse hydropic degeneration of hepatocytes compared with the normal group, but severe liver lesions in all experimental rats in group 3 (Hepatic carcinoma induction group) ranged from inflammation, fibrosis till carcinomas induction compared with normal and drug supplement groups, while in the prevention group displayed mild-to-moderate lesions and few cases showed early carcinomas development in comparison with group 3 and finally, in group 5 MO/asc.-Se-NPs drug treatment noticed tissue improvements and diminished lesions through showed only a few reversible degenerative changes as diffuse hydropic degeneration of hepatocytes in the hepatic parenchyma. Overall, our study focused on hepatocellular carcinoma induced with carbon tetrachloride (CCl_4) and thioacetamide (TAA) which both caused stimulation of hepatic tissue damage through elevation of oxidative stress and reactive oxygen species (ROS) may excite the concentration of oxidative cell which the equilibrium between antioxidant capability and ROS was jumbled forming DNA damage and leading to oxidative stress in hepatocytes, through the accumulated fat droplets in cytoplasm and pushing the nucleus to periphery of hepatocytes the inflammation began to appear which consists of (neutrophils, eosinophils, lymphocytes and Kupffer cells) followed by fibrosis and cirrhosis are progressively became series main pathological features and presence of atypical hepatocytes with hemorrhaging and ischemic necrosis in tumor with losing of lobular architecture squeezing the surrounding parenchyma and development of HCC which increase through the experiment in group 3 after 8 weeks through histological examination While in group 4 which take the drug 3 h before CCL_4 induction showed less infection than group 3 but after 4 weeks of treatment with MO /asc.-Se-NPs platform drug group 5 observed more improvement by showing restricted small areas of hyperchromatic divided nuclei within normal hepatic parenchyma.

Methods

All chemicals and reagents were purchased from Merck co. (Kenilworth, New Jersey, USA). Kits used for biochemical analysis in liver purchased from well-known brands manufactured in USA. Rat IL-6 (Interleukin 6) ELISA Kit, Catalog No: E-EL-R0015 (Elabscience Biotechnology, United states). Malonaldehyde (MDA) colorimetric assay kit, catalog No: E-BC-K025-S (Elabscience Biotechnology, United states). HR-TEM (Ted Pella, Redding, CA, USA), DLS (BIC, USA and PCS), Zetasizer (Beckman Coulter, Miami, FL, USA) were used for characterization of *MO*/asc.-Se NP. Technetium-99m was obtained from RPF, EAEA, Egypt. NaI (Tl) γ-counter (SPECTECH, ST450 SCA, USA) for radioactivity measuring. All data were expressed as mean ± SD. The groups were compared using one-way ANOVA, where $P < 0.05$ was considered significant.

Preparation of *Moringa oleifera* leaves methanol extract

Fresh *Moringa oleifera* leaves were cordially obtained from the Egyptian Scientific Society of Moringa (ESSM). The plant was identified and authenticated by botanists in National Research Centre, Egypt. *MO* leaves were washed several times with distilled water to remove needless material then dried in a shadow for one month. Then it grounded by a mortar/pestle to produce a fine powder. 500 gm from the dark greenish

powder separated and mixed with 4L MeOH (HPLC grade). The mixture was sonicated for 1 h then left to macerate at room temperature in the dark for 3 days. The mixture was filtered for removing insoluble materials then the solvent was evaporated under vacuum at 50 °C yielding 77 g of dark greenish residue. All these steps were repeated twice for removal any remaining residue.

HPLC analysis of *Moringa oleifera* leaves methanol extract

HPLC analysis was carried out using Agilent Technologies 1100 series liquid chromatograph equipped with an auto sampler and a diode-array detector. The analytical column was an Eclipse XDB-C18 (150 X 4.6 μm; 5 μm) with a C18 guard column (Phenomenex, Torrance, CA). The mobile phase consisted of acetonitrile (solvent A) and 2% acetic acid in water (v/v) (solvent B). The flow rate was kept at 0.8 ml/min for a total run time of 70 min and the gradient program was as follows: 100% B to 85% B in 30 min, 85% B to 50% B in 20 min, 50% B to 0% B in 5 min and 0% B to 100% B in 5 min. The injection volume was 50 μl and peaks were monitored simultaneously at 280 and 320 nm for the benzoic acid and cinnamic acid derivatives, respectively. All samples were filtered through a 0.45-μm Acrodisc syringe filter (Gelman Laboratory, MI) before injection. Peaks were identified by congruent retention times and UV spectra and compared with those of the standards (Kim et al. 2006).

Synthesis and characterization of *MO*/asc.-Se-NPs

Firstly; a solution of 22.70 mM ascorbic acid was added to 5.00 mM sodium selenite in a ratio of 1:1, then mixed and left at room temperature for 30 min forming asc.-Se-NPs. Secondly; asc.-Se-NPs was added to *MO* extract with a concentration of 3.25 mg/mL in a ration 1:1 forming *MO*/asc.-Se-NPs just after 15 min. *MO*/asc.-Se-NPs platform was well characterized using HR-TEM for shape detection and core diameter determination, DLS for determination of hydrodynamic diameter and zeta-sizer for determination the zeta-potential of the formed nanoplatform.

Antioxidant capacity determination of MO /asc.-Se-NPs

Sodium selenite, ascorbic acid and *Moringa* extract were prepared in concentrations of 5, 22.7 and 2 mg/mL, respectively. *MO*/asc.-Se-NPs was prepared by mixing 1.5 mL from each solution forming final volume of 4.5 mL. The tested samples are: 4.5 mL from *MO*/asc.-Se-NPs and 1.5 mL from sodium selenite, ascorbic acid and *Moringa* extract each of them completed to final volume of 4.5 mL.

a) DPPH assay

Free radicals scavenging activity was determined thorough 2,2-diphenyl-1-picryl-hydrazyl-hydrate (DPPH) assay (Boly et al. 2016) to compare between selenium, *Moringa oleifera* methanol extract, ascorbic acid and *MO*/asc.-Se-NPs according to its effective on antioxidant capacity, First 100μL of freshly prepared DPPH reagent (0.1% in methanol) then add 100 μL of sample in wells plate, after incubation in dark place at room temperature for 30 min. the density of the reaction color was measured at 540 nm using

microplate reader FluoStar Omega and the result was represented by the following equation:

$$\%RSA = \frac{\mathrm{A0} - A1}{A0} \times 100,$$

where RSA is the radical scavenging activity, A0 is the absorbance of control and A1 is the absorbance of test.

b) Superoxide dismutase (SOD)

Superoxide anion radical scavenging activity assay was based on the reduction of nitro blue tetrazolium (NBT) in the presence of NADH and phenazonium methosulphate (PMS) under aerobic condition (Nishikimi et al. 1972; Verma et al. 2009).

Radiosynthesis of [^{99m}Tc]Tc-*MO*/asc.-Se-NPs

[^{99m}Tc]Tc-MO /asc.-Se-NPs was synthesized by optimizing many factors MO/asc.-Se-NPs, $SnCl_2$. $2H_2O$, pH and time to give the best RCP (radio chemical purity). The reaction was monitored via paper chromatography technique and % RCP was determined using mixture (ammonia:ethanol:water 1:2:5) and acetone as mobile phases for colloid and free pertechnetate determination, respectively (Motaleb ad Sakr 2011; Sakr et al. 2013).

Pharmacokinetic study [^{99m}Tc]Tc-*MO*/asc.-Se-NPs

Ain Shams university Ethical Committee number (213/16–02-2022) approved the biodistribution studies following the European Community guidelines associated with Directive 2010/63/EU (Abdulwahab et al. 2020). Swiss Albino mice aged three months weight 20–25 g were divided into 6 groups (n = 3). [^{99m}Tc]Tc-*MO*/asc.-Se-NPs was injected intravenously, then the mice were anaesthetized using chloroform then weighed and dissected at different times (15, 30, 60, 120, 180 and 360 min) post-injection. Blood, bones and muscles were freshly collected and weighed then assumed to its ratio in the body (7%, 10%, and 40%, respectively) (Motaleb et al. 2017; Swidan et al. 2015, 2014). All the other organs of interest were also collected and counted by using a gamma counter for determination of radioactivity. % Injected dose/gram (%ID/g) was used calculated for each.

In vivo application of *MO*/asc.-Se-NPs

Induction of liver hepatocellular carcinoma

The hepatocellular carcinoma was induced in rats by intra-peritoneal injection of CCl_4 diluted with corn oil in ratio (1:1) with dose (1 mL/1 kg) weekly for 12 weeks, where at the same time they received (0.3 gm/L) of thioacetic acid (TAA) in drinking water every day (Heindryckx et al. 2009).

Experiment protocol

In this study, 50 (6-week-old) male Wister Albino rats were used. Rats were taken as a gift from the animal house of Egyptian Atomic Energy Authority. The rats weighed about

200 ± 10 g. Rats were housed in suitable cages and kept under stable environmental conditions with 25 ℃ temperature and equal dark/light cycle and they supplied regularly by food and water. The animals were kept for 2 weeks under these conditions before beginning in the experimental protocol. Rats were divided into 5 groups (10 rats for each) and the following protocol was applied.

Weeks	**Groups**				
	Control normal group (1) (rats received no drugs)	***MO*/asc.-Se-NPs supplement group (2) (rats received weekly dose of *MO*/asc.-Se-NPs)**	**HCC induction group (3) (cancer induction group without treatment)**	**Prevention group (4) (rats received weekly dose of *MO*/asc.-Se NPs in parallel with the induction protocol of HCC induction group)**	**Treatment group (5) (treatment course after HCC induction)**
1,2,3,4,5, 6,7,8,9,10, 11, and 12	Rats received no drugs, served as control non-treated	* IP injection of *MO*/asc.-Se NPs(1 mL/kg) (once a week)	* IP injection of CCl_4 soln. (1 mL/kg) (once a week) * TAA (0.3 gm/L) in drinking water daily	* IP injection of *MO*/asc.-Se-NPs(1 mL/kg) * After 3 h. IP injection of CCl_4 soln. (1 mL/kg) (once a week) * TAA (0.3 gm/L) in drinking water daily	* IP injection of CCl_4 soln. (1 mL/kg) (once a week) * TAA (0.3 gm/L) in drinking water daily
	*Samples collection *Biochemical and histopathological studies				
13,14,15, and 16					* IP injection of *MO*/asc.-Se-NPs (1 mL/kg) (once a week) * Samples collection * Biochemical and histopathological stud

*This protocol was selected according to previously used protocols (Aljuhr et al. 2021; Uehara et al. 2014b) with some modifications. The duration was selected according to weekly biomedical analysis and comparison with control

Sampling

Exactly after 12 weeks from the application of experimental protocol on murines, all groups were killed except group 5 which was killed after 4 more weeks. Blood samples were collected in plain tube for serum liver function tests alanine aminotransferase (ALT), aspartate aminotransferase (AST), and albumin (Alb), a lobe of liver collected in 10% formalin for histological investigation, anther lobe rinsed in phosphate-buffered saline, and weighed, after which it was homogenized and centrifuged at 15,000 rpm for 10 min at 4 °C and stored at − 80 °C for analysis.

Evaluation of serum biochemical parameters

The serum was obtained by centrifuging the blood samples at 4000 rpm for 10 min to obtain serum. The serum levels of the liver injury biomarkers (AST, ALT, and Alb) were measured using Human kit (Germany) by Systronics Spectrophotometer

following the manufacturer's instructions. The reaction of AST based on combination of α-oxoglutarate with L-aspartate forming oxaloacetate and L-glutamate which reaction further with NADH to form L-malate and NAD+. The activity of ALT kinetically predestined the mechanism based on α-oxoglutarate and L-alanine reaction catalyzed by ALT to form L-glutamate and pyruvate. albumin has been greatly simplified by the introduction of dye binding method albumin at pH 4.2 is sufficiently cationic to bind the anionic dye bromocresol green (BCG) to form a blue-green colored complex.

Liver homogenate preparation

Fresh tissue of liver was washed with PBS (0.01 M, pH 7.4) to remove blood cells and weight then homogenized at the ratio of the volume of homogenized medium to the weighted tissue homogenate 9 mL:1 g. the homogenate was centrifuged for 10 min at 10,000*g* at 4 °C. The supernatant was taken in ice for detection.

Analysis of inflammatory cytokines in the liver

400 mL of liver homogenate was inserted with 400 mL 0.2% phosphoric acid then discrete into two glass tubes equally. The levels of inflammatory interleukin 6 (IL-6) in the liver homogenates using Rat IL-6 ELISA Kit. Micro ELISA plate pre-coated with an antibody specific to Rat IL-6. Homogenate sample was added to wells (100uL for each well) for 90 min at 37℃. Aspirate and wash 5 times washed with Dilute 30 mL of concentrated wash buffer with 720 mL of deionized to prepare 750 mL. Then 350 µL was added to each well. Soak for 1 ~ 2 min and decant the solution from each well and pat it dry against clean absorbent paper. This wash step was repeated 3 times, and add 100 µL of HRP conjugate (a biotinylated detection antibody specific for Rat IL-6 and avidin-horseradish peroxidase (HRP)) and incubated for 30 min at 37℃. Then wash for wash buffer for 5 times, after that 90 µL substrate reagent was added. The color appeared blue then incubated for 15 min at 37℃. Stop solution 50 µL was added which turned the color into yellow which immediately the optical density (OD) is measured spectrophotometrically at a wavelength of 450 nm ± 2 nm. The OD value is proportional to the concentration of Rat IL-6. The concentration of Rat IL-6 in the samples was calculated by comparing the OD of the samples to the standard curve.

Evaluation of liver lipid peroxidation and antioxidant biomarkers (MDA assay)

Thiobarbituric acid assay Kit (TBARS) was used to appreciate reactive oxygen species (ROS) by measuring the end product of lipid peroxidation, malondialdehyde (MDA) (Halliwell and Chirico 1993).

Malondialdehyde (MDA) Colorimetric Assay Kit, catalog No: E-BC-K025-S, (Elabscience Biotechnology, United states) was used as the following steps:

(a) Preparing four tubes (blank, standard, sample, and control) as following:

Blank tube: X mL of absolute ethanol into the 10 mL glass test tubes.

Standard tube: X mL of 10 nmol/mL Standard into the 10 mL glass test tubes.

Sample tube: X mL of tested sample (10% rat liver tissue homogenate) into numbered 10 mL glass test tubes.

Control tube: X mL of tested sample into numbered 10 mL glass test tubes.

(b) Add X mL of reagent 1 into each tube of Step (a).
(c) Add 3 mL of reagent 2 application solution into each tube of Step (b).
(d) Add 1 mL of reagent 3 application solution into blank tube, standard tube, sample tube, add 1 mL of 50% glacial acetic acid (≥ 99.5%) into control tube.
(e) Mix fully and fasten the mouth of the tube with plastic film, prick a small hole with a needle. Then incubate the tubes at 95–100℃ for 40 min.
(f) Cool the tubes to room temperature with running water, centrifuge the tubes at 3100 g for 10 min.
(g) Take 3 mL the supernatant of each tube. Set the spectrophotometer to zero with double distilled water and measure the OD value at 532 nm with 1 cm optical path cuvette.

$$MDAcontent(nmol/mgprot) = \frac{\Delta A_1}{\Delta A_2} \times c \times f \div C_{pr}$$

Note: ΔA_1: $OD_{Sample} - OD_{Control}$, ΔA_2: $OD_{Standard} - OD_{Blank}$, c: The concentration of standard, 10 nmol/mL, f: dilution factor of sample before tested, and C_{pr}: concentration of protein in sample, mgprot/mL.

Histopathological examination

Pathological changes in livers samples were demonstrated through paraffin technique at which livers samples were fixed with 10% neutral formaldehyde buffer, dehydrated by degraded concentrations of alcohol, cleared in xylol then embedded in paraffin wax and cut into 4-µm-thick sections and finally applied hematoxylin–eosin (HE) staining for histopathological examination (Suvarna et al. 2018) using a light microscope using 400× magnification power. The tissue sections were subjected to blinded microscopic examination, and the abnormal tissue alteration records were scored according to previously reported studies (Al-Sayed et al. 2019; El-Nabarawy et al. 2020).

Conclusion

MO possesses many components with excellent health benefits including antioxidant and anticancer properties. Keeping in view the anticancer properties of MO, we hypothesized it may be a more effective treatment for HCC in the form of nanoparticles. To achieve the maximum benefits from *MO* extract, we used the synergistic effect of selenium and MO components in a nanoplatform. We focused our study on revealing and proving the hepatoprotective, antioxidant and anti-inflammatory face of Se-NPs. The pharmacokinetic study of *MO*/asc.-Se-NPs was performed via radiolabeling with ^{99m}Tc. The presented study has succeeded in developing a novel platform

of selenium nanoparticles capped with *MO* leaves extract in an acceptable nano-size range. The results in this study suggested that *MO*/asc.-Se-NPs show a valuable protective and treatment tool for use as a therapy for the treatment of HCC.

Acknowledgements
Not applicable.

Author contributions
EMME performed the experiments and wrote the original draft. AAS designed the experimental protocols, participated in the practical part and analyzed the results and was a contributor in writing the manuscript. GHS, GNAG, KEA and AAS are supervisors for this study and revised the manuscript. All authors read and approved the final manuscript.

Funding
Open access funding provided by The Science, Technology & Innovation Funding Authority (STDF) in cooperation with The Egyptian Knowledge Bank (EKB).

Availability of data and materials
Not applicable.

Declarations

Ethics approval and consent to participate
Ain Shams University Ethical Committee approved this animal biodistribution studies.

Consent for publication
Not applicable.

Competing interests
The authors declare that they have no competing interests.

Author details
[1]Chemistry Department, Faculty of Science, Ain Shams University, AbbassiaCairo 11566, Egypt. [2]Provincial Lab. 44511, Animal Health Research Institute, Zagazig, Sharkia, Egypt. [3]Labeled Compounds Department, Hot Laboratories Centre, Egyptian Atomic Energy Authority (EAEA), Cairo 13759, Egypt.

Received: 18 March 2022 Accepted: 7 May 2022
Published online: 21 May 2022

References

Abdulwahab HG, Harras MF, El Menofy NG, Hegab AM, Essa BM, Selim AA et al (2020) Novel thiobarbiturates as potent urease inhibitors with potential antibacterial activity: Design, synthesis, radiolabeling and biodistribution study. Bioorg Med Chem 28(23):115759

Akbari B, Baghaei-Yazdi N, Bahmaie M, MahdaviAbhari F (2022) The role of plant-derived natural antioxidants in reduction of oxidative stress. BioFactors 23:14

Akhter T (2023) To study the composition of minerals and vitamins of some fresh vegetables with special reference to the Kullu District of Himachal Pradesh India. Sustaina Agri Food Environ Res 12:1

Aljuhr SA, Abdelaziz G, Essa BM, Zaghary WA, Sakr TM (2021) Hepatoprotective, antioxidant and anti-inflammatory potentials of Vit-E/C@ SeNPs in rats: Synthesis, characterization, biochemical, radio-biodistribution, molecular and histopathological studies. Bioorg Chem 117:105412

Al-Sayed E, Abdel-Daim MM, Khattab MA (2019) Hepatoprotective activity of praecoxin A isolated from Melaleuca ericifolia against carbon tetrachloride-induced hepatotoxicity in mice Impact on oxidative stress, inflammation, and apoptosis. Phytother Res 33(2):461–470

Alsohaimi IH, Nassar AM, Elnasr TAS, amar Cheba, B. (2020) A novel composite silver nanoparticles loaded calcium oxide stemming from egg shell recycling: a potent photocatalytic and antibacterial activities. J Clean Prod 248:119274

Ati VM, Meye ED, Refli AO, Amalo D, Jebatu UL (2022) Moringa leaf (Moringa oleifera L) flavonoids utilization in suppressing growth of Aedes aegypti larvae Pemanfaatan Flavonoid Daun Kelor (Moringa oleifera L) dalam Menekan Pertumbuhan Larva Nyamuk Aedes aegypti. Jurnal Ilmiah Berkala: Sains Dan Terapan Kimia 16:1

Augustine R, Hasan A, Primavera R, Wilson RJ, Thakor AS, Kevadiya BD (2020) Cellular uptake and retention of nanoparticles: Insights on particle properties and interaction with cellular components. Materials Today Commun 25:101692

Bai K, Hong B, Hong Z, Sun J, Wang, C.J.J.o.n. (2017) Selenium nanoparticles-loaded chitosan/citrate complex and its protection against oxidative stress in D-galactose-induced aging mice. J Immunol 15(1):1–14

Bergmann J, Müller M, Baumann N, Reichert M, Heneweer C, Bolik J et al (2017) IL-6 trans-signaling is essential for the development of hepatocellular carcinoma in mice. Develop Sign 65(1):89–103

Bhondave PD, Devarshi PP, Mahadik KR, Harsulkar AMJJ (2014) 'Ashvagandharishta'prepared using yeast consortium from Woodfordia fruticosa flowers exhibit hepatoprotective effect on CCl4 induced liver damage in Wistar rats. RATS 151(1):183–190

Boly R, Lamkami T, Lompo M, Dubois J, Guissou I (2016) DPPH free radical scavenging activity of two extracts from Agelanthus dodoneifolius (Loranthaceae) leaves. Int J Toxicol Pharmacol Res 8(1):29–34

Brar S, Haugh C, Robertson N, Owuor PM, Waterman C, Fuchs GJ III et al (2022) The impact of Moringa oleifera leaf supplementation on human and animal nutrition, growth, and milk production: A systematic review. Phytother Res 12:78
Choi SI, Cho Y, Ki M, Kim BH, Lee IJ, Kim TH et al (2022) Better survival of patients with hepatitis B virus-related hepatocellular carcinoma in South Korea: Changes in 16-years cohorts. PLoS ONE 17(3):e0265668
Choudhari AS, Mandave PC, Deshpande M, Ranjekar P, Prakash OJF (2020) Phytochemicals in cancer treatment: From preclinical studies to clinical practice. Clinics J 10:1614
Chung I-M, Rekha K, Rajakumar G, Thiruvengadam M (2018) Elicitation of silver nanoparticles enhanced the secondary metabolites and pharmacological activities in cell suspension cultures of bitter gourd. Biotech 8(10):1–12
Ciumărnean L, Milaciu MV, Runcan O, Vesa ŞC, Răchişan AL, Negrean V et al (2020) The effects of flavonoids in cardiovascular diseases. Molecules 25(18):4320
de Siqueira Patriota LL, Ramos, D.d.B.M., Dos Santos, A.C.L.A., Silva, Y.A., e Silva, M.G., Torres, D.J.L., et al (2020) Antitumor activity of Moringa oleifera (drumstick tree) flower trypsin inhibitor (MoFTI) in sarcoma 180-bearing mice. Food Chem Toxicol 145:111691
Domenicali M, Baldassarre M, Giannone FA, Naldi M, Mastroroberto M, Biselli M et al (2014) Posttranscriptional Changes of Serum Albumin: Clinical and Prognostic Significance in Hospitalized Patients with Cirrhosis. Biotech 60(6):1851–1860
Dutta S, Sengupta P, Slama P, Roychoudhury S (2021) Oxidative stress, testicular inflammatory pathways, and male reproduction. Int J Mol Sci 22(18):10043
Elbakry MA, El Rabey HA, Elremaly W, Sakran MI, Almutairi FMJBR (2019) The methanolic extract of Moringa oleifera attenuates CCl4 induced hepatonephro toxicity in the male rat. Biomed Res 30(1):23–31
El-Nabarawy NA, Gouda AS, Khattab MA, Rashed LA (2020) Effects of nitrite graded doses on hepatotoxicity and nephrotoxicity, histopathological alterations, and activation of apoptosis in adult rats. Environ Sci Pollut Res 27(12):14019–14032
Essa BM, El-Mohty AA, El-Hashash MA, Sakr TM (2020) 99mTc-citrate-gold nanoparticles as a tumor tracer: synthesis, characterization, radiolabeling and in-vivo studies. Radiochim Acta 108(10):809–819
Fakurazi S, Hairuszah I, Nanthini UJF, toxicology, c. (2008) Moringa oleifera Lam prevents acetaminophen induced liver injury through restoration of glutathione level. Food Technol Res 46(8):2611–2615
Fayez H, El-Motaleb MA, Selim AA (2020) Synergistic cytotoxicity of shikonin-silver nanoparticles as an opportunity for lung cancer. J Labelled Compd Radiopharm 63(1):25–32
Fitriana WD, Istiqomah SBT, Ersam T, Fatmawati S (2018) The relationship of secondary metabolites: A study of Indonesian traditional herbal medicine (Jamu) for post partum maternal care use. In: AIP Conference Proceedings (Vol. 2049, pp. 020096): AIP Publishing LLC
Fontana R, Macchi G, Caproni A., Sicurella M., Buratto M., Salvatori F., et al. (2022). Control of Erwinia amylovora Growth by Moringa oleifera Leaf Extracts: In Vitro and in Planta Effects. *Plants, 11*(7), 957.
Garcia-Martinez, R., Caraceni, P., Bernardi, M., Gines, P., Arroyo, V., & Jalan, R.J.H. (2013). Albumin: pathophysiologic basis of its role in the treatment of cirrhosis and its complications. *58*(5), 1836–1846.
Ghosh, J., Sil, P.C., Manna, P., & Das, J. (2010). Contribution of type 1 diabetes to rat liver dysfunction and cellular damage via activation of NOS, PARP, IκBα/NF-κB, MAPKs, and mitochondria-dependent pathways: Prophylactic role of arjunolic acid.
Gong X, Smith JR, Swanson HM, Rubin LP (2018) Carotenoid lutein selectively inhibits breast cancer cell growth and potentiates the effect of chemotherapeutic agents through ROS-mediated mechanisms. Molecules 23(4):905
Halliwell B, Chirico SJTA (1993) Lipid peroxidation: its mechanism, measurement, and significance. Am J Clin Res 57(5):715S-725S
Heindryckx F, Colle I, Van Vlierberghe HJI (2009) Experimental mouse models for hepatocellular carcinoma research. Int J Pathol 90(4):367–386
Johnson ITJP (2007) Phytochemicals and cancer. Proc Nutr Soc 66(2):207–215
Katz L, Baltz RHJJ, Biotechnology F (2016) Natural product discovery: past, present, and future. Jind Microbiol Biotechnol 43(2–3):155–176
Kim K-H, Tsao R, Yang R, Cui SWJFC (2006) Phenolic acid profiles and antioxidant activities of wheat bran extracts and the effect of hydrolysis conditions. Food Chem 95(3):466–473
Korany M, Mahmoud B, Ayoub SM, Sakr TM, Ahmed SA (2020) Synthesis and radiolabeling of vitamin C-stabilized selenium nanoparticles as a promising approach in diagnosis of solid tumors. J Radioanal Nucl Chem 325(1):237–244
Kornek M, Raskopf E, Guetgemann I, Ocker M, Gerceker S, Gonzalez-Carmona MA et al (2006) Combination of systemic thioacetamide (TAA) injections and ethanol feeding accelerates hepatic fibrosis in C3H/He mice and is associated with intrahepatic up regulation of MMP-2, VEGF and ICAM-1. J Hepatol 45(3):370–376
Lahkar M, Thakuria BJIP, Sciences A (2012) Comparative study of the hepatoprotective activities of Vitex Negundo linn and Moringa oleifera lam in paracetamol induced hepatotoxicity in experimental animals. J Heptol 2(5):74–79
Leone A, Spada A, Battezzati A, Schiraldi A, Aristil J, Bertoli SJI (2016) Moringa oleifera seeds and oil: Characteristics and uses for human health. Int J Mol Sci 17(12):2141
Li Y, Guo M, Lin Z, Zhao M, Xia Y, Wang C et al (2018) Multifunctional selenium nanoparticles with Galangin-induced HepG2 cell apoptosis through p38 and AKT signalling pathway. R Soc Open Sci 5(11):180509
Lin X, Huang R, Zhang S, Zheng L, Wei L, He M et al (2012) Methyl helicterate protects against CCl4-induced liver injury in rats by inhibiting oxidative stress, NF-κB activation, Fas/FasL pathway and cytochrome P4502E1 level. Food Chem Toxicol 50(10):3413–3420
Malhotra S, Welling M, Mantri S, Desai KJB (2016) In vitro and in vivo antioxidant, cytotoxic, and anti-chronic inflammatory arthritic effect of selenium nanoparticles. J Imflamm 104(5):993–1003
Meireles D, Gomes J, Lopes L, Hinzmann M, Machado J (2020) A review of properties, nutritional and pharmaceutical applications of Moringa oleifera: integrative approach on conventional and traditional Asian medicine. Adv Tradit Med 20(4):495–515

Menon S, Ks SD, Santhiya R, Rajeshkumar S, Kumar VJC, Biointerfaces SB (2018) Selenium Nanoparticles: A Potent Chemotherapeutic Agent and an Elucidation of Its Mechanism 170:280–292
Mgbojikwe AC, Samuel KV, Olanihan AO, Okeke-Agulu KI, Okpara JO (2022) The evaluation of the anticoccidial properties of aqueous leaf extract of Moringa oleifera. Food Environ Safety J 20:4
Moichela FT (2021) In vitro effects of aqueous leaf extracts of moringa oleifera on human sperm.
Motaleb M, Sakr T (2011) Synthesis and preclinical pharmacological evaluation of 99mTc-TEDP as a novel bone imaging agent. J Labelled Compd Radiopharm 54(9):597–601
Motaleb M, Selim AA, El-Tawoosy M, Sanad M, El-Hashash M (2017) Synthesis, radiolabeling and biological distribution of a new dioxime derivative as a potential tumor imaging agent. J Radioanal Nucl Chem 314(3):1517–1522
Motaleb M, Selim AA, El-Tawoosy M, Sanad M, El-Hashash M (2018) Synthesis, characterization, radiolabeling and biodistribution of a novel cyclohexane dioxime derivative as a potential candidate for tumor imaging. Int J Radiat Biol 94(6):590–596
Muriel P (2009) Role of free radicals in liver diseases. Mol Mech 3(4):526–536
Naugler WE, Karin MJT (2008) The wolf in sheep's clothing: the role of interleukin-6 in immunity, inflammation and cancer. J Imflamm 14(3):109–119
Nazir, I., & Gangoo, S.A. (2022). Pharmaceutical and Therapeutic Potentials of Essential Oils.
Newman DJ, Cragg G (2020) Natural products as sources of new drugs over the nearly four decades from 01/1981 to 09/2019. *83*(3), 770–803.
Nie T, Wu H, Wong K-H, Chen TJJ (2016) Facile synthesis of highly uniform selenium nanoparticles using glucose as the reductant and surface decorator to induce cancer cell apoptosis. Cell 4(13):2351–2358
Nishikimi M, Rao NA, Yagi K (1972) The occurrence of superoxide anion in the reaction of reduced phenazine methosulfate and molecular oxygen. Biochem Biophys Res Commun 46(2):849–854
Okorie C, Ajibesin K, Sanyaolu A, Islam A, Lamech S, Mupepi K et al (2019) A review of the therapeutic benefits of Moringa oleifera in controlling high blood pressure (hypertension). Curr Tradit Med 5(3):232–245
Pereira JM, Viell FLG, de Lima PC, Silva E, Pilau EJ, Correa RC et al (2021) Optimization of the extraction of antioxidants from Moringa leaves: A comparative study between ultrasound-and ultra-homogenizer-assisted extractions. J Food Process Preserv 45(6):e15512
Rodriguez EOC (2020) Chemical proximate composition, antinutritional factors content, and antioxidant capacity of anatomical seed fractions of Moringa oleifera.
Safitri H, Restu W, Cencelya VC, Fadila W, Witri RE (2022) Analysis Of Red Spinach (Amaranthus Tricolor) As An Antioxidant. Extra Teritorial 1(01):24–29
Sakr T, Moustapha M, Motaleb M (2013) 99mTc-nebivolol as a novel heart imaging radiopharmaceutical for myocardial infarction assessment. J Radioanal Nucl Chem 295(2):1511–1516
Sakr TM, Korany M, Katti KV (2018) Selenium nanomaterials in biomedicine—An overview of new opportunities in nanomedicine of selenium. J Drug Deliv Sci Technol 46:223–233
Sakr TM, El-Hashash M, El-Mohty A, Essa BM (2020) 99mTc-gallic-gold nanoparticles as a new imaging platform for tumor targeting. Appl Radiat Isot 164:109269
Salama MA, El Harkaoui S, Nounah I, Sakr H, Abdin M, Owon M et al (2020) Oxidative stability of Opuntia ficus-indica seeds oil blending with Moringa oleifera seeds oil☆. OCL 27:53
Schacherer D, Schoelmerich J, Zuber-Jerger, I.J.Z.f.G. (2007) The diagnostic approach to hepatocellular carcinoma. Diagn 45(10):1067–1074
Shamsel-Din HA, Gizawy MA, Abdelaziz G (2020) Molecular docking and preliminary bioevaluation of 99m Tc-Thiadiazuron as a novel potential agent for cervical cancer imaging. J Radioanal Nucl Chem 326(2):1375–1381
Sharma A, Khanna S, Kaur G, Singh I (2021) Medicinal plants and their components for wound healing applications. Fut J Pharma Sci 7(1):1–13
Shimoda H, Tanaka J, Kikuchi M, Fukuda T, Ito H, Hatano T et al (2008) Walnut polyphenols prevent liver damage induced by carbon tetrachloride and d-galactosamine: hepatoprotective hydrolyzable tannins in the kernel pellicles of walnut. J Agric Food Chem 56(12):4444–4449
Soliman NI, El-Desouky M, Nahas AE-HAE-M (2021) Cypermethrin-induced lung damage in albino rats: the preventive impact of *Moringa oleifera*. Egypt J Chem 64(10):3–4
Susanto A, Muhaimina RK, Amaliya A, Sutjiatmo AB (2019) The effectiveness of ethanolic extract of Moringa Leaves (Moringa oleífera Lam) Gel on the Wound Healing Process of the Rat's Palate. J Int Dental Med Res 12(2):504–509
Suvarna KS, Layton C, Bancroft JD (2018) Bancroft's theory and practice of histological techniques. Elsevier Health Sciences, New York
Swidan M, Sakr T, Motaleb M, El-Bary AA, El-Kolaly M (2014) Radioiodinated acebutolol as a new highly selective radiotracer for myocardial perfusion imaging. J Labelled Compd Radiopharm 57(10):593–599
Swidan M, Sakr T, Motaleb M, El-Bary A, El-Kolaly M (2015) Preliminary assessment of radioiodinated fenoterol and reproterol as potential scintigraphic agents for lung imaging. J Radioanal Nucl Chem 303(1):531–539
Tajuddeen N, Van Heerden FRJ (2019) Antiplasmodial natural products: an update. Nature 18(1):1–62
Thomas D, KurienThomas K, Latha M (2020) Preparation and evaluation of alginate nanoparticles prepared by green method for drug delivery applications. Int J Biol Macromol 154:888–895
Uehara T, Pogribny IP, Rusyn IJC (2014a) The DEN and CCl4-induced mouse model of fibrosis and inflammation-associated hepatocellular carcinoma. Curr Protocols Pharmacol 66(1):10
Verma AR, Vijayakumar M, Mathela CS, Rao CV (2009) In vitro and in vivo antioxidant properties of different fractions of Moringa oleifera leaves. Food Chem Toxicol 47(9):2196–2201
Vonghirundecha P, Chusri S, Meunprasertdee P, Kaewmanee T (2022) Microencapsulated functional ingredients from a Moringa oleifera leaf polyphenol-rich extract: Characterization, antioxidant properties, in vitro simulated digestion, and storage stability. LWT 154:112820
Wijaya FAT (2019). Research and development final project "moringa spread (low calories and high in protein)": ottimmo international mastergourmet academy.

Xia Y, Zhong J, Zhao M, Tang Y, Han N, Hua L et al (2019) Galactose-modified selenium nanoparticles for targeted delivery of doxorubicin to hepatocellular carcinoma. Target 26(1):1–11
Yeshi K, Crayn D, Ritmejerytė E, Wangchuk P (2022) Plant secondary metabolites produced in response to abiotic stresses has potential application in pharmaceutical product development. Molecules 27(1):313
Zhou W, Yang L, Nie L, Lin H (2021) Unraveling the molecular mechanisms between inflammation and tumor angiogenesis. Am J Cancer Res 11(2):301

Publisher's Note